

Highly sensitive and stable SERS probes of alternately deposited Ag and Au layers on 3D SiO_2nanogrids for detection of trace mercury ions

Yi Tian(田毅), Han-Fu Wang(王汉夫), Lan-Qin Yan(闫兰琴), Xian-Feng Zhang(张先锋), Attia Falak, Pei-Pei Chen(陈佩佩), Feng-Liang Dong(董凤良), Lian-Feng Sun(孙连峰), Wei-Guo Chu(褚卫国)

Citation: Chin. Phys. B . 2018, 27(7): 077406. **doi:** 10.1088/1674-1056/27/7/077406

Journal homepage: http://cpb.iphy.ac.cn; http://iopscience.iop.org/cpb

What follows is a list of articles you may be interested in

The structure and elasticity of phase B silicates under high pressure by first principles simulation

Lei Liu(刘雷), Li Yi(易丽), Hong Liu(刘红), Ying Li(李营), Chun-Qiang Zhuang(庄春强), Long-Xing Yang(杨龙星), Gui-Ping Liu(刘桂平)

Chin. Phys. B . 2018, 27(4): 047402. **doi:** 10.1088/1674-1056/27/4/047402

High-pressure synchrotron x-ray diffraction and Raman spectroscopic study of plumbogummite

Duan Kang(康端), Xiang Wu(巫翔), Guan Yuan(袁冠), Sheng-Xuan Huang(黄圣轩), Jing-Jing Niu(牛菁菁), Jing Gao(高静), Shan Qin(秦善)

Chin. Phys. B . 2018, 27(1): 017402. **doi:** 10.1088/1674-1056/27/1/017402

Quantitative analysis of ammonium salts in coking industrial liquid waste treatment process based on Raman spectroscopy

Ya-Nan Cao(曹亚南), Gui-Shi Wang(王贵师), Tu Tan(谈图), Ting-Dong Cai(蔡廷栋), Kun Liu(刘锟), Lei Wang(汪磊), Gong-Dong Zhu(朱公栋), Jiao-Xu Mei(梅教旭)

Chin. Phys. B . 2016, 25(10): 107403. **doi:** 10.1088/1674-1056/25/10/107403

First-principles simulation of Raman spectra and structural properties of quartz up to 5 GPa

Liu Lei, Lv Chao-Jia, Zhuang Chun-Qiang, Yi Li, Liu Hong, Du Jian-Guo

Chin. Phys. B . 2015, 24(12): 127401. **doi:** 10.1088/1674-1056/24/12/127401

Perforated nanocap array: Facile fabrication process and efficient surface enhanced Raman scattering with fluorescence suppression

Wang Jun, Huang Li-Qing, Tong Hui-Min, Zhai Li-Peng, Yuan Lin, Zhao Li-Hua, Zhang Wei-Wei, Shan Dong-Zhi, Hao Ai-Wen, Feng Xue-Hong

Chin. Phys. B . 2013, 22(4): 047301. **doi:** 10.1088/1674-1056/22/4/047301

Highly sensitive and stable SERS probes of alternately deposited Ag and Au layers on 3D SiO_2 nanogrids for detection of trace mercury ions*

Yi Tian(田毅)[1,2], Han-Fu Wang(王汉夫)[1], Lan-Qin Yan(闫兰琴)[1], Xian-Feng Zhang(张先锋)[1], Attia Falak[1,2], Pei-Pei Chen(陈佩佩)[1,†], Feng-Liang Dong(董凤良)[1,‡], Lian-Feng Sun(孙连峰)[1,2,§], and Wei-Guo Chu(褚卫国)[1,2,¶]

[1] *CAS Key Laboratory for Nanosystems and Hierachical Fabrication, Nanofabrication Laboratory, CAS Center for Excellence in Nanoscience, National Center for Nanoscience and Technology, Beijing* 100190, *China*

[2] *University of Chinese Academy of Sciences, Beijing* 100049, *China*

(Received 11 May 2018; published online 25 June 2018)

The hazard of Hg ion pollution triggers the motivation to explore a fast, sensitive, and reliable detection method. Here, we design and fabricate novel 36-nm-thick Ag–Au composite layers alternately deposited on three-dimensional (3D) periodic SiO_2 nanogrids as surface-enhanced Raman scattering (SERS) probes. The SERS effects of the probes depend mainly on the positions and intensities of their localized surface plasmon resonance (LSPR) peaks, which is confirmed by the absorption spectra from finite-difference time-domain (FDTD) calculations. By optimizing the structure and material to maximize the intrinsic electric field enhancement based on the design method of 3D periodic SERS probes proposed, high performance of the Ag–Au/SiO_2 nanogrid probes is achieved with the stability further enhanced by annealing. The optimized probes show the outstanding stability with only 4.0% SERS intensity change during 10-day storage, the excellent detection uniformity of 5.78% (RSD), the detection limit of 5.0×10^{-12} M (1 ppt), and superior selectivity for Hg ions. The present study renders it possible to realize the rapid and reliable detection of trace heavy metal ions by developing high-performance 3D periodic structure SERS probes by designing novel 3D structure and optimizing plasmonic material.

Keywords: surface-enhanced Raman scattering, Ag–Au composite layer, nanostructure design, trace Hg ions detection

PACS: 74.25.nd, 73.90.+f, 78.30.–j, 78.67.–n **DOI:** 10.1088/1674-1056/27/7/077406

1. Introduction

It is well known that mercury is a highly toxic pollutant that can do harms to human health even at a very low concentration due to the bio-concentration.[1,2] At present, several methods, such as atomic absorption spectrometry,[3] atomic fluorescence spectrometry,[4] X-ray fluorescence spectrometry,[5] and inductively coupled plasma mass spectroscopy[6] have been proposed for the detection of mercury. However, these methodologies are time-consuming and tedious, and thus it is quite necessary to develop a fast, sensitive, and reliable detection method of Hg ion residues. Surface-enhanced Raman scattering (SERS) is a very powerful technique for molecule detection which has extensive applications in chemical, biological and environmental fields with a low limit of detection.[7–11]

The detection limit of SERS probes does mean something especially for trace or single molecule detection, which is primarily dependent on the maximum intrinsic electromagnetic field (EMF) produced on plasmonic substrates.[12] So far, the main methods to improve the detection limit is by reducing the gaps at hot spots and/or utilizing coupling effects between surface plasmon polaritons (SPPs) and localized surface plasmon resonance (LSPR) in some specific nanostructures.[13–16] In addition, bimetallic composite nanostructures like Ag–Au nanoparticles have presented higher SERS activity than the nanoparticles made from either pure silver or gold.[17–20] Meanwhile, bimetallic Ag–Au materials have the potential to combine the advantages of both metals, i.e., higher SERS activity of Ag,[21,22] better biocompatibility, and chemical stability of Au.[23,24] Improving the stability of the SERS probes is beneficial to the reproducibility of signals, which is significant for the practical application.

Herein, we developed novel three-dimensional (3D) periodic Ag–Au/SiO_2 hybrid SERS probes by electron beam evaporating alternately Ag and Au with different thickness ratios on 3D periodic hexagonal SiO_2 nanogrids combining annealing treatment for exploration of SERS activity and sta-

*Project supported by the National Key Research and Development Program of China (Grant No. 2017YFA0207104), the Strategic Priority Research Program of the Chinese Academy of Sciences (Grant No. XDA09040101), the National Natural Science Foundation of China (Grant No. Y6061111JJ), the Youth Innovation Promotion Association of Chinese Academy of Sciences (Grant No. 2015030), and the Key Technology Talent Program of Chinese Academy of Sciences (Grant Nos. Y8482911ZX and Y7602921ZX).

†Corresponding author. E-mail: chenpp@nanoctr.cn

‡Corresponding author. E-mail: dongfl@nanoctr.cn

§Corresponding author. E-mail: slf@nanoctr.cn

¶Corresponding author. E-mail: wgchu@nanoctr.cn

© 2018 Chinese Physical Society and IOP Publishing Ltd

bility. Based on the general design principles for the 3D periodic nanostructures SERS probes we proposed,[25] we designed the optimized sizes for Ag–Au SERS probes. The optimized SERS probes show the strongest intrinsic electric field enhancement, which is demonstrated by SERS experiments. The SERS activity of Ag–Au/SiO_2 nanogrid probes with a certain thickness ratio of Ag and Au is stronger than that of pure Ag and Au structures with the same total thickness under the excitation of a 514 nm laser, which can be explained by the relative positions and intensities of LSPR absorption peaks of these probe structures. The optimized probes show the superior sensitivity, stability, uniformity, and selectivity which were successfully applied to the detection of trace Hg ions in water.

2. Experimental

2.1. Design and fabrication of Ag–Au/SiO_2 nanogrids

Three-dimensional (3D) Ag–Au/SiO_2 periodic nanogrids with various thickness ratios of Ag and Au were designed and fabricated. Hydrogen silsesquioxane (HSQ XR-1541–006, Dow Corning, USA) was firstly spin-coated on silicon (100) substrates with the thickness of 198 nm. Patterning was realized by using electron beam lithography (EBL, Vistec EBPG 5000 plus ES, Raith Company, Germany) with an accelerating voltage of 100 kV and a beam current of 2 nA, followed by the development. The typical width of SiO_2 sidewalls for all nanogrids was controlled to be around 11 nm (Fig. A1).[26,27] Alternate deposition of Ag and Au with m cycles, along with a 1-nm-thick Cr adhesion layer was performed on an electron-beam evaporator (OHMIKER-50B, Cello-Tech Company, Taiwan, China) with the constant total thickness of 36 nm. The rate of deposition was 0.4 Å/s for Cr and 0.2 Å/s for both Ag and Au. The fabricated structures were observed using a scanning electron microscope (NOVA NanoSEM 430, FEI Company, USA). Upon annealing, the samples were heated to 200 °C at a rate of 10 °C/min and kept for 1 h in nitrogen in a fast alloy furnace (RTP3, Shentong-TOEC Company, China), followed by cooling down to room temperature.

2.2. Optical measurements and FDTD calculations

The optical constants of Ag–Au composite layers were determined using a spectroscopic ellipsometer (SE 850 DUV, Sentech Company, Germany). Finite- difference time-domain (FDTD) method was used to calculate the absorption spectra and spatial distributions of the electromagnetic fields. For simplicity, we used the rough Ag–Au/SiO_2 models with periodically arranged semiellipsoid-like Ag–Au composite nanoparticles with a smooth Ag–Au composite film of 2 nm thick on the sidewalls of SiO_2 nanogrids to model the real Ag–Au/SiO_2 nanogrids in which the sizes and center distance of particles were semi-principal axes, $a = b = 20.0$ nm, $c = 10.0$ nm, and $d = 40.0$ nm for the calculations of absorption spectra.[25] The width and height of SiO_2 grids were 11 and 198 nm, respectively. The structures were illuminated with a plane wave with x-direction linear polarization incident along the –z axis. Periodic boundary conditions for the xz and yz planes were applied to simulate an infinite array of periodic nanogrids or nanowalls. Perfectly matched layer (PML) boundary conditions were used in the z-direction. The mesh size used in the simulation region was 2 nm for the calculations of absorption spectra and 0.5 nm for the calculations of the electromagnetic fields.

2.3. SERS measurements for detection of Hg ions

The samples were first immersed into 4,4'-Bipyridine (Bpy) absolute ethanol solution with a concentration of 10^{-5} M for 4 h, and then dried naturally in air as SERS probes for Hg ions detection. 35 μL of Hg ion solutions with different concentrations of 5.0×10^{-12} (1 ppt), 5.0×10^{-11} (10 ppt), 5.0×10^{-9}, 5.0×10^{-7}, and 5.0×10^{-5} M were dropped onto the SERS probes, respectively, then kept for 10 min, and finally dried in air. Likewise, 35 μL deionized water was prepared with the same procedure as SERS probes for the blank control group. The SERS measurements were performed using a 514 nm laser with a power of 0.5 mW and the x-polarization on a Raman microscope (Renishaw inVia, Renishaw company, UK) equipped with a 20× objective (NA = 0.4) and an integration time of 10 s. For each sample, measurements on at least five different positions were taken.

3. Results and discussion

3.1. Effect of Au–Ag composite materials on the SERS signal

We designed and fabricated alternate Ag and Au layers with various thicknesses deposited on hexagonal 3D periodic SiO_2 nanogrids with a total thickness of 36 nm to maximize the SPP effects based on the proposed design method for exploration of SERS activity and stability.[25] Here, 2-nm-thick Ag and 2-nm-thick Au deposited alternately on hexagonal SiO_2 nanogrids with a grid length of 188 nm and a height of 198 nm for 9 cycles is labeled by (2 nm Ag–2 nm Au)-9c/198 nm SiO_2_h188. The scanning electron microscopy (SEM) images of these samples are shown in Fig. 1, which reveals Ag–Au nanoparticles to form the rough sidewalls of nanogrids and the roughness of sidewalls appears to be very similar for Ag–Au layers with different thickness ratios. The statistical analysis of SEM images shown in Fig. 1 gives the almost same average widths of hybrid nanogrids with different atomic percents of Ag of about 28 nm with about 8.5-nm-thick Ag–Au layers on each side of about 11-nm-thick SiO_2 nanogrids, as shown in Fig. A1.

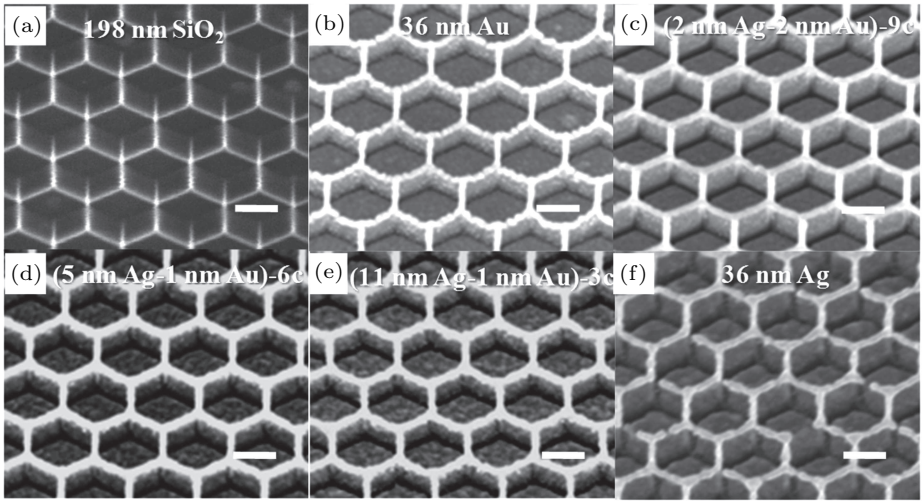


Fig. 1. Tilt SEM images of SiO_2 and hybrid hexagonal nanogrids_h188 with a height of 198 nm. (a) SiO_2 nanogrids. (b) 36 nm Au/SiO_2 nanogrids. (c) (2 nm Ag–2 nm Au)-9c/SiO_2 nanogrids. (d) (5 nm Ag–1 nm Au)-6c/SiO_2 nanogrids. (e) (11 nm Ag–1 nm Au)-3c/SiO_2 nanogrids. (f) 36 nm Ag/SiO_2 nanogrids. Scale bars: 200 nm.

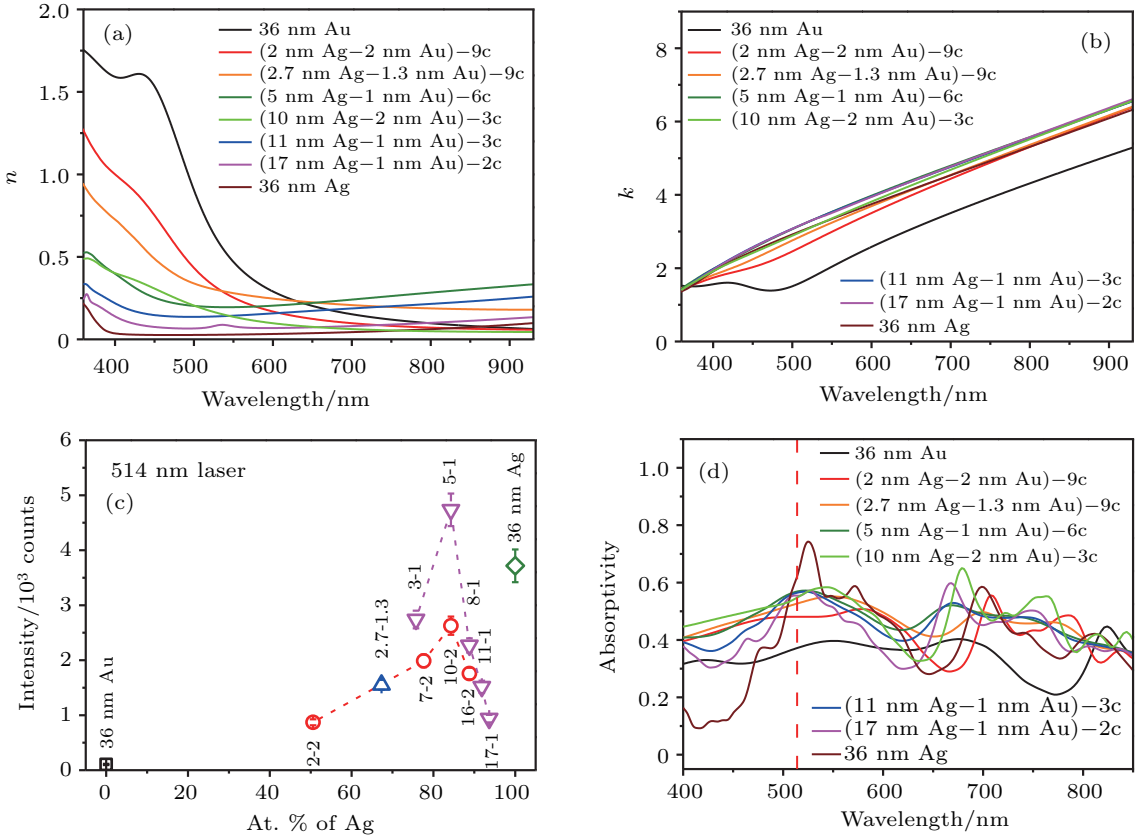


Fig. 2. (color online) (a), (b) Refractive indexes and extinction coefficients of different Ag–Au composite layers derived from the measurements by spectroscopic ellipsometry, respectively. (c) Changes of experimental Raman intensities of the peak positioned at 1610 cm^{-1} of the Bpy-decorated 36 nm Ag–Au/198 nm SiO_2 nanogrids_h188 with different thickness ratios of Ag and Au (atomic percentage of Ag) for 514 nm wavelength laser. (d) The calculated absorption spectra of 36 nm Ag–Au/198 nm SiO_2 nanogrids_h188 with different thickness ratios of Ag and Au.

In order to obtain optical properties of the Ag–Au composite layers above, their equivalent refractive indexes n and extinction coefficients k within the wavelength range from 360 nm to 930 nm were derived by fitting the spectroscopic ellipsometric curves using effective medium approximation method (EMA),[28] as shown in Figs. 2(a) and 2(b), respectively. It is evident that the equivalent optical constants change with Ag–Au composite layers even for the thickness ratio of Ag to Au, such as (5 nm Au-1 nm Ag)-6c and (10 nm Au-2 nm Ag)-3c.

To evaluate the performance, the Raman intensity of the peak at 1610 cm^{-1} of Bpy molecules is recorded to investigate SERS activity here, and its dependences on atomic ratio of Ag for 36 nm Ag–Au/198 nm SiO_2 nanogrids_h188 are presented in Fig. 2(c). The intensity is found to firstly increase more rapidly with the increase of Ag proportion and reach the maxi-

mum at 84.3% (i.e., (5 nm Ag-1 nm Au)-6c), and then decrease gradually but increase suddenly for pure Ag, indicative of the material properties dependences. Interestingly, the intensity of the (10 nm Ag–2 nm Au)-3c sample is found to be far lower than that of (5 nm Ag–1 nm Au)-6c sample though with the same percentage of Ag atoms. We believe that the SERS signal intensities were mainly related to their LSPR peaks which depend on the optical properties of materials (Figs. 2(a) and 2(b)) and structures. LSPRs are excited at the gaps between bottom and sidewalls, and at those on rough sidewalls under the light illumination, but those on the bottom film are negligible due to the weak electric field enhancements.[25]

To get plasmon resonance modes for the hybrid structures with different Ag–Au components, we performed finite-difference time-domain (FDTD) simulations to derive the corresponding absorption spectra by assuming the same sidewall roughness and using the measured equivalent optical constants. The results are shown in Fig. 2(d) from which we can see three groups of peaks in the spectra. For the 36 nm Au/SiO_2 structure, one of the absorption peaks is near 675 nm and blue shifts to 523 nm with the increase of Ag atomic ratio. With the Ag atomic ratio above 84% (i.e., (5 nm Ag–1 nm Au)-6c), the position of the peak changes little but its intensity decreases. For the 36 nm Ag/SiO_2 structure, the resonance peak red shifts slightly but its intensity increases significantly. In addition, the resonance peak of the (10 nm Ag–2 nm Au)-3c structure red shifts a little compared with the (5 nm Ag–1 nm Au)-6c structure. Therefore, the changes of the absorption peak intensity under excitation of 514 nm laser can explain the Ag atomic ratio dependence of the experimental Raman intensity well.

3.2. Size optimization for Au–Ag/SiO_2 nanogrids

For periodic and rough Ag–Au/SiO_2 hybrid nanogrids, SPP waves and their interference effects, LSPR effects, standing wave effect of incident light and coupling effects between LSPR and SPP are involved.[25] For 514 nm light, a height with 36% of the incident light wavelength, 185 nm, is adequate for the strongest intrinsic EMF enhancement due to the standing wave effect (the height here is 198 nm which can meet the condition).[25] The interference effects of SPP waves due to Fabry Perot (FP)-like resonance caused by multiple reflections in periodic structures,[29,30] can excite LSPR as a secondary source (incident light as primary sources), like Au/SiO_2 nanogrid structures.[25] According to the calculation formula of SPP wavelength and the equivalent optical constants of the Ag–Au composite layers (Figs. 2(a) and 2(b)),[31] the wavelengths of SPP waves excited at these metal/air interfaces for the 514 nm excitation light are shown in Table A1. The SPP wavelengths range from 474 nm to 488 nm for Ag–Au composite layers with different thickness ratios, with 485 nm for the pure Ag and 375 nm for the pure Au. Here, we employ 488 nm for structure design.

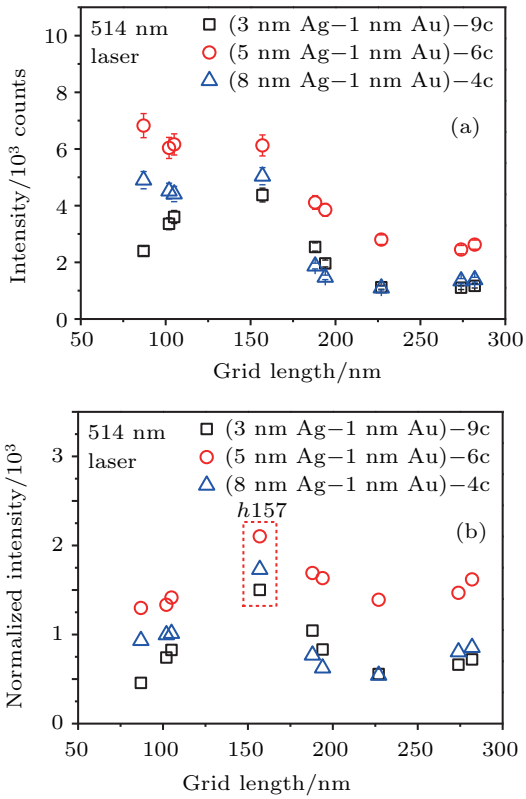


Fig. 3. (color online) (a) Changes of experimental SERS intensities of hexagonal Ag–Au/198 nm SiO_2 nanogrids with different thickness ratios of Ag and Au against grid length for 514 nm laser. (b) Changes of their corresponding normalized SERS intensities.

The general design principles for 3D structures also hold for Ag–Au/SiO_2 nanogrids structures here.[25] It is known that the SPP interference effects depend mainly on the geometries of structure especially the sidewall spacing (materials independent) and the reflectance of SPP wave reflected by the sidewall (materials dependent).[25] Therefore, we need to know the sidewall spacing dependence of LSPR and the reflectance for Ag–Au/SiO_2 nanogrids. Taking (5 nm Ag–1 nm Au)-6c/198 nm SiO_2 as an example, sidewall spacing L_w dependences of the maximum and averaged $|E/E_0|^4$ from LSPR on the rough nanowalls at TE mode calculated by FDTD solutions are given in Fig. A2. The maximum and average electric field enhancements ($|E/E_0|^4$) are both maximized at $L_w \sim 300$ nm. Its reflectance of SPP wave, $R = 0.46$ calculated by FDTD on the model with 8.5-nm-thick Ag–Au composite layers on each side of SiO_2 sidewall for the 488 nm SPP wave, is larger than that of 36 nm Au/SiO_2 sidewall, $R = 0.29$, implying the stronger interference intensity of SPP wave in Ag–Au/SiO_2 nanogrids compared to Au/SiO_2 nanogrids. Therefore, the geometric dimension dependence of SPP wave interference effect (FP-like resonance) still plays a dominant role in the relationship between the total electric field enhancement and the size of the Ag–Au/SiO_2 nanogrids. The hexagonal

Ag–Au/SiO_2 nanogrids with the sidewall spacing of half SPP wavelength is the optimum structure with the strongest intrinsic electric field enhancement, which will be confirmed by the following SERS experiments.

SEM image of the optimized hexagonal 36 nm Ag–Au/198 nm SiO_2 nanogrids_h157 samples with 28 nm sidewall width and 244 nm sidewall spacing (half of 488 nm SPP wavelength) is compared with those h87, h101, h105, h188, h194, h227, h274, and h282, as shown in Fig. A3. Their SERS intensities and corresponding normalized intensities are shown in Figs. 3(a) and 3(b), respectively. Both the intensity and normalized intensity of the (5 nm Ag–1 nm Au)-6c/198 nm SiO_2 nanogrids SERS probe are the largest compared to those of (3 nm Ag–1 nm Au)-9c, (5 nm Ag–1 nm Au)-6c and (8 nm Ag–1 nm Au)-4c with the same grid length, which is attributed to the positions and intensities of the absorption peaks as discussed above (Fig. 2(d)). With the grid length, the normalized intensity shows the quasi-periodic characteristics and reaches the maximum at h157 for three kinds of Ag–Au structures, which indicates the maximum intrinsic electric field enhancement of h157. This reveals that our design method for 3D periodic SERS probes is generalized which can be applied to different materials.[25]

3.3. Stability improvement and Hg ions detection

In order to study the detection performances of the Ag–Au and Ag/SiO_2 nanogrid SERS probes for Hg ions, SERS measurements were conducted on the SERS probes onto which Hg ion solutions with different concentrations were dropped. Meanwhile, deionized water instead of Hg ion solutions was prepared as the blank control experiments with the same procedure. The intensity changes of Ag–Au and Ag/SiO_2 nanogrid probes with the concentration of Hg ions and their SEM images after SERS measurements are shown in Fig. A4. The probes with the higher percentages of Au, such as the pure Au[25] and (2 nm Ag–2 nm Au)-9c samples are not sensitive enough to the extremely low Hg ions concentrations, and thus their detection limits are only 5.0×10^{-11} M. Their morphologies changed little after SERS measurements. In sharp contrast, the morphology of the pure Ag probe underwent significant changes after Hg ion detection, and its detection limit is also only 5.0×10^{-11} M with a poorly linear relationship between intensity variations and concentrations which should be attributed to the instability of Ag in the atmosphere.[32] For the (5 nm Ag–1 nm Au)-6c and (11 nm Ag–1 nm Au)-3c/SiO_2 nanogrid probes, their detection limits for Hg ions are 5.0×10^{-12} M (1 ppt) with the linear relationships between intensity variations and Hg concentrations. This indicates that the Ag–Au composite layers with proper configurations would show the strengths of high sensitivity Ag and the high stability of Au simultaneously, which is therefore of great significance for practical applications.

We found that the change of signal intensity for (10 nm Ag–2 nm Au)-3c/SiO_2 nanogrids probe during the storage of 10 days is smaller than that of (5 nm Ag–1 nm Au)-6c/SiO_2 nanogrids probe, which indicates the better stability with 2 nm Au surface layer. Based on this, we fabricated (7 nm Ag–2 nm Au)-4c and (16 nm Ag–2 nm Au)-2c/198 nm SiO_2 nanogrids_h157 probes with 2 nm thick Au outermost layer to study the stability of the unannealed and annealed probes after 10 days of storage. We annealed the Au, Ag, and Ag–Au/198 nm SiO_2 nanogrids structures, and their SEM images are shown in Fig. 4. We found that the changes of morphologies for structures with thickness ratios of Ag and Au less than 8:1 after annealed are not obvious, but those of the structures with a higher percentage of Ag are significant. These SERS probes annealed were also used to detect the Hg ions, without obvious changes of morphologies, indicating that the annealing treatment makes the SERS probes more stable.

Experimental SERS intensities of unannealed and annealed hexagonal (2 nm Ag–2 nm Au)-9c, (7 nm Ag–2 nm Au)-4c, and (16 nm Ag–2 nm Au)-2c/198 nm SiO_2 nanogrids_h157 probes are shown in Fig. 5(a). Their SERS intensities changed by -34.7%, 27.7%, and 24.4% after annealing. Relative intensity changes of unannealed, annealed, and 10-day stored hexagonal 36 nm Ag–Au/198 nm SiO_2 nanogrid probes with different thickness ratios of Ag and Au are shown in Fig. 5(b). The SERS intensity for the pure Au probe stored for 10 days decreased by 32.2%, possibly related to the surface adsorption of C, O, S, and other elements.[33] The SERS intensity for the Ag–Au probes with higher percentages of Ag increased significantly by 200%–370% after 10 days of storage, which is mainly due to the formation of silver sulfide on silver during the exposure to air.[32] Exposure to air for a short time would lead to a Ag_2S layer as thin as about 1 nm which could enhance the average electric field at hot spots dramatically. However, the longer time exposure would increase the thickness of Ag_2S layer,[32] decreasing the average electric field enhancement greatly again, as demonstrated by FDTD calculations in Fig. A5. In addition, few changes of SERS intensities for the Ag–Au composite layers with proper proportions of Ag changed little after 10 days of storage are considered to probably result from a synergistic effect of the enhancement effect caused by a thin Ag_2S layer and the weakening effect caused by the adsorption of C, O, S and other elements. Again, for the same atomic ratios of Ag the intensities for the probes with a 2-nm-thick Au outermost layer changed less than those a 1-nm-thick Au outermost layer, which is mainly due to the better stability of Au.[24] Therefore, increasing the thickness of outermost Au layer may facilitate the stability of probes. It can also be observed that annealing leads to the less change of intensity for SERS probes after 10- day storage,

which stabilizes the probes by releasing the stress and stabilizing the microstructure.[34] By comparison, annealed (7 nm Ag–2 nm Au)-4c/198 nm SiO_2 nanogrids_h157 probe shows both the highest intensity and the best stability with only 4.0% change in SERS intensity after 10-day storage, as illustrated in Fig. 5(a).

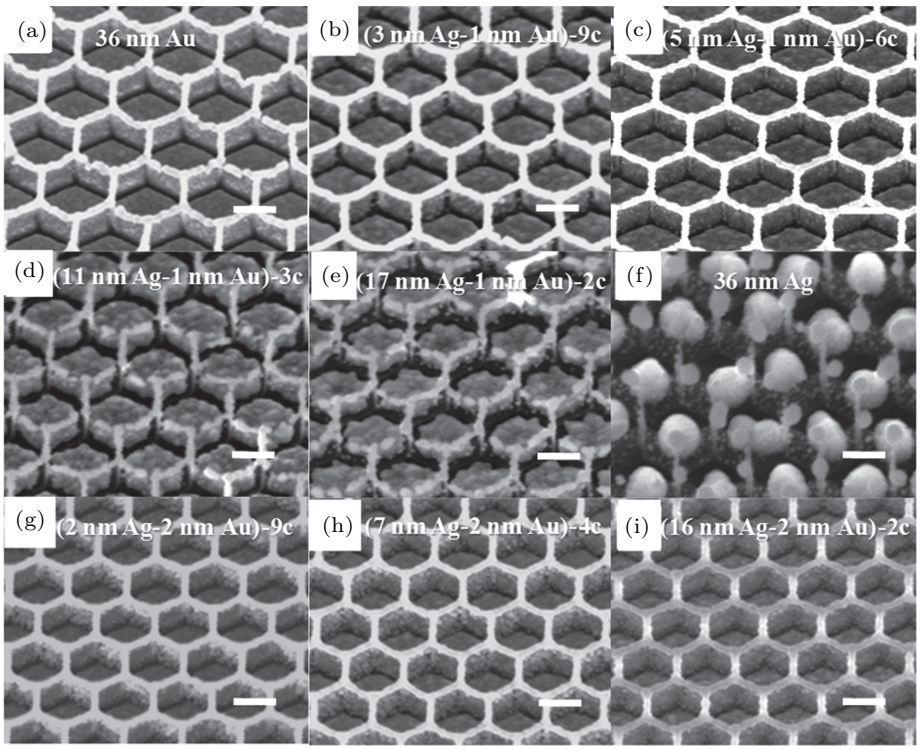


Fig. 4. Tilt SEM images of annealed Au, Ag–Au and Ag/198 nm SiO_2 nanogrids. (a)–(f) 36 nm Au, (3 nm Ag–1 nm Au)-9c, (5 nm Ag–1 nm Au)-6c, (11 nm Ag–1 nm Au)-3c, (17 nm Ag–1 nm Au)-2c, and 36 nm Ag/198 nm SiO_2_h188, respectively. (g)–(i) (2 nm Ag–2 nm Au)-9c, (7 nm Ag–2 nm Au)-4c, and (16 nm Ag–2 nm Au)-2c/198 nm SiO_2_h157, respectively. Scale bars: 200 nm.

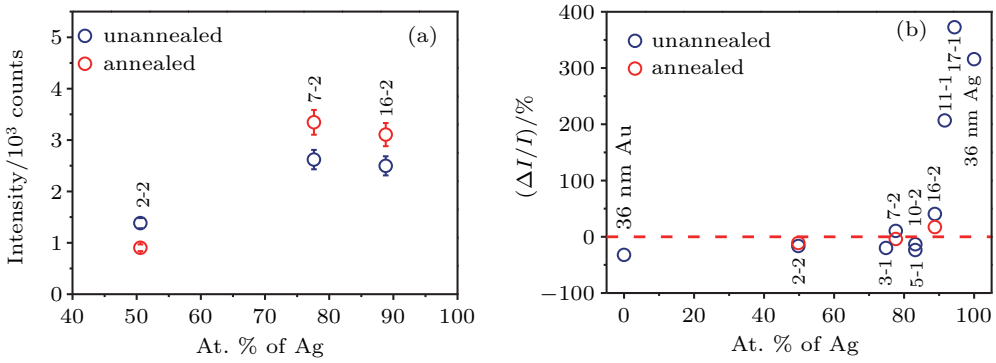


Fig. 5. (color online) (a) Experimental SERS intensities of annealed and unannealed hexagonal Ag–Au/198 nm SiO_2 nanogrids with different Ag and Au thickness ratios. (b) Relative changes of SERS intensities of the above probes stored for 10 days.

Here, the annealed hexagonal (7 nm Ag–2 nm Au)-4c/198 nm SiO_2 nanogrids_h157 SERS probes with 10-day and without storage (0 day) were used to detect Hg ions, as shown in Figs. 6(a) and 6(b), respectively. The relationships between intensity variation and the concentration (5.0×10^{-12} M to 5.0×10^{-5} M) for both probes are found to be linear (Figs. 6(a) and 6(b)). Both probes detected 5.0×10^{-12} M (1 ppt) trace Hg ions in water successfully, which is outstanding among those reported, about three orders of magnitude lower than the US threshold value (10 nM or 2000 ppt) for drinkable water.[35,36] The SERS mapping of the annealed probe gives a low RSD of 5.78% (Fig. 6(c)), normally much smaller than those of the reported SERS substrates,[13,37,38] which is quite significant for SERS probes. The excellent selectivity of the optimized SERS probes to Hg ions shown in Fig. 6(d) was demonstrated by comparing with other metal ions with the same concentration of 10^{-6} M, such as Mg^{2+}, Co^{2+}, Ni^{2+}, Li^{+}, Cu^{2+}, Zn^{2+}, Fe^{3+}, Al^{3+}, In^{3+}, Mn^{2+}, Pb^{2+}, and mixed (without and with Hg ions) metal ions. The superior selectivity of the probes renders it possible to be applied for practical detections of trace Hg ions.

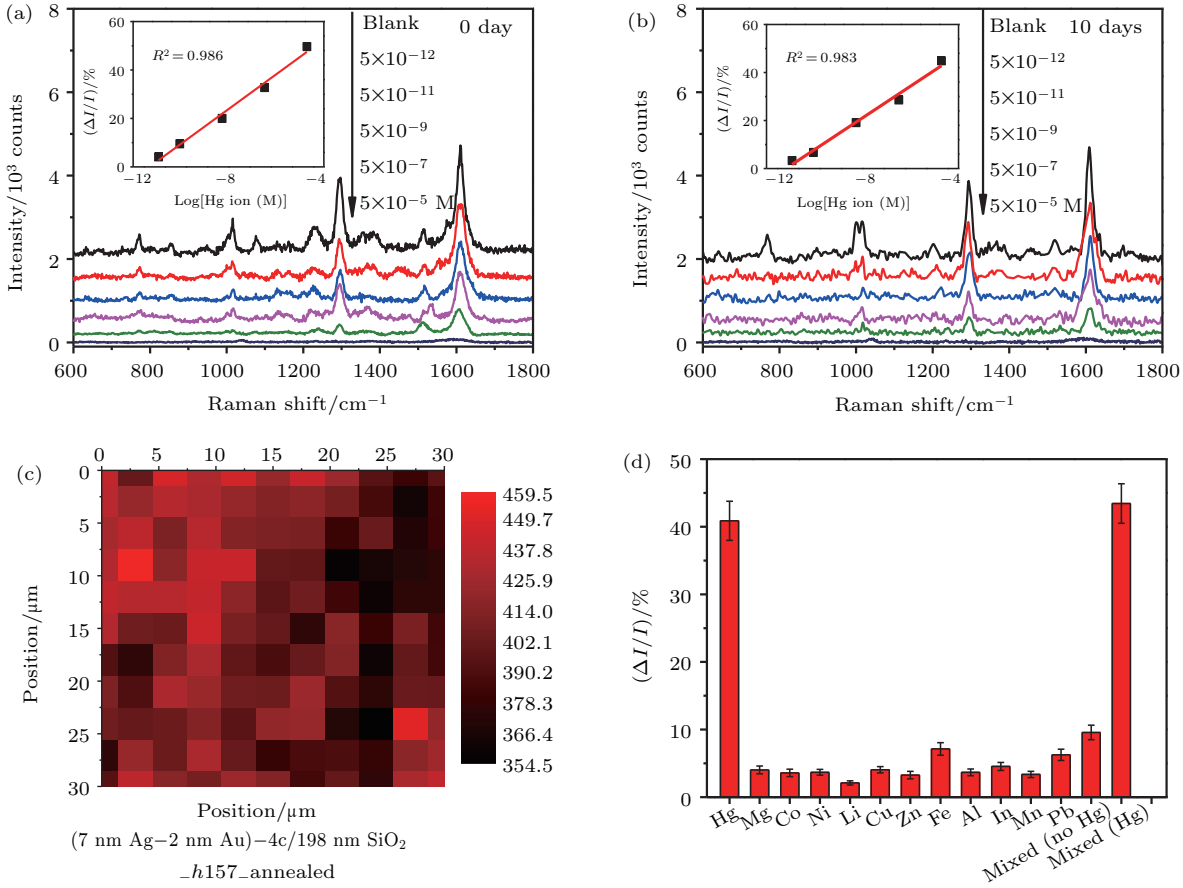


Fig. 6. (color online) (a), (b) Detection of Hg ions by the annealed (7 nm Ag–2 nm Au)-4c/198 nm SiO_2 nanogrids_h157 probes stored for 0 and 10 days, respectively. Raman spectra of Bpy molecules and the relationships between Raman signal intensities and concentrations of Hg ions. (c) Raman intensity mapping of the annealed hexagonal (7 nm Ag–2 nm Au)-4c/198 nm SiO_2 nanogrids_h157 decorated by Bpy as SERS probes. (d) Selectivity of the optimized SERS probes for the detection of Hg ions over other metal ions.

4. Conclusion and perspectives

In summary, we designed and fabricated novel 3D periodic Ag–Au/SiO_2 nanogrids as SERS probes for trace Hg ions detection. High performances were realized by structural optimization in terms of maximization of electric field enhancement at hot spots responsible for SERS effects, and material optimization, i.e., deposition of alternate Au and Ag layers on SiO_2 nanogrids with different thickness ratios and a total thickness of 36 nm. Annealing is demonstrated to favor stabilizing SERS probes. The SERS effects of the probes are related to not only the positions and intensities of their LSPR peaks but the Ag and Au proportions at the surface, which was basically confirmed by the absorption spectra derived from FDTD calculations. The design method of 3D periodic SERS probes proposed based on plasmonic gold proves to hold for not only single constituent plasmonic materials but also plasmonic composite materials such as Ag–Au composite layers here.[25] By structural optimization the annealed (7 nm Ag–2 nm Au)-4c/198 nm SiO_2 nanogrids_h157 probes show the best stability with only 4.0% SERS intensity change during 10-day storage, good detection uniformity (RSD 5.78%), the detection limit of 5.0×10^{-12} M (1 ppt), and superior selectivity of detection for Hg ions. Therefore, the combination of structural design and material optimization makes it possible to develop novel 3D periodic structures as high-performance SERS probes which can be applied to rapid and reliable detection of trace heavy ion such as trace Hg ions in water.

Appendix A

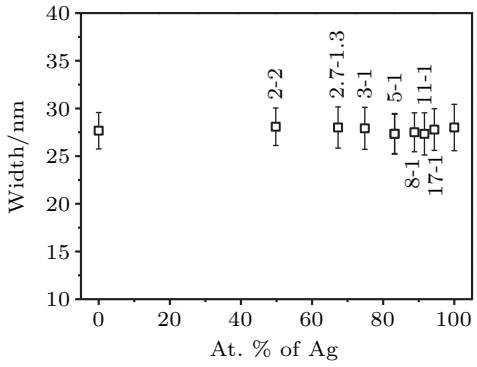


Fig. A1. Width of 36 nm Ag–Au/198 nm SiO_2 nanogrids with different Ag and Au thickness ratios.

Table A1. Relative permittivities ε_m and calculated SPP wavelengths λ_{SPP} of Ag–Au composite layers with different Ag and Au thickness ratios for 514 nm excitation light.

Metals	ε_m	λ_{SPP}/nm
36 nm Au	–2.144	375.44
(2 nm Ag–2 nm Au)-9c	–6.658	473.83
(2.7 nm Ag–1.3 nm Au)-9c	-8.296	482.03
(5 nm Ag–1 nm Au)-6c	–10.215	488.19
(10 nm Ag–2 nm Au)-3c	–9.078	484.86
(11 nm Ag–1 nm Au)-3c	–10.270	488.33
(17 nm Ag–1 nm Au)-2c	–10.286	488.38
36 nm Ag	-9.261	485.46

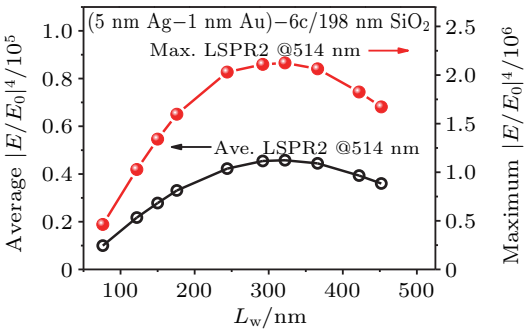


Fig. A2. (color online) The calculated average and maximum localized electric field enhancements of (5 nm Ag–1 nm Au)-6c/198 nm SiO_2 nanogrids with various sidewall spacings for TE mode under the excitation of a 514 nm laser, respectively, in which the sizes and center distance of particles were semi-principal axes, $a = b = 6.5$ nm, $c = 8.0$ nm, and $d = 13.3$ nm for the calculations of the electromagnetic fields.[25]

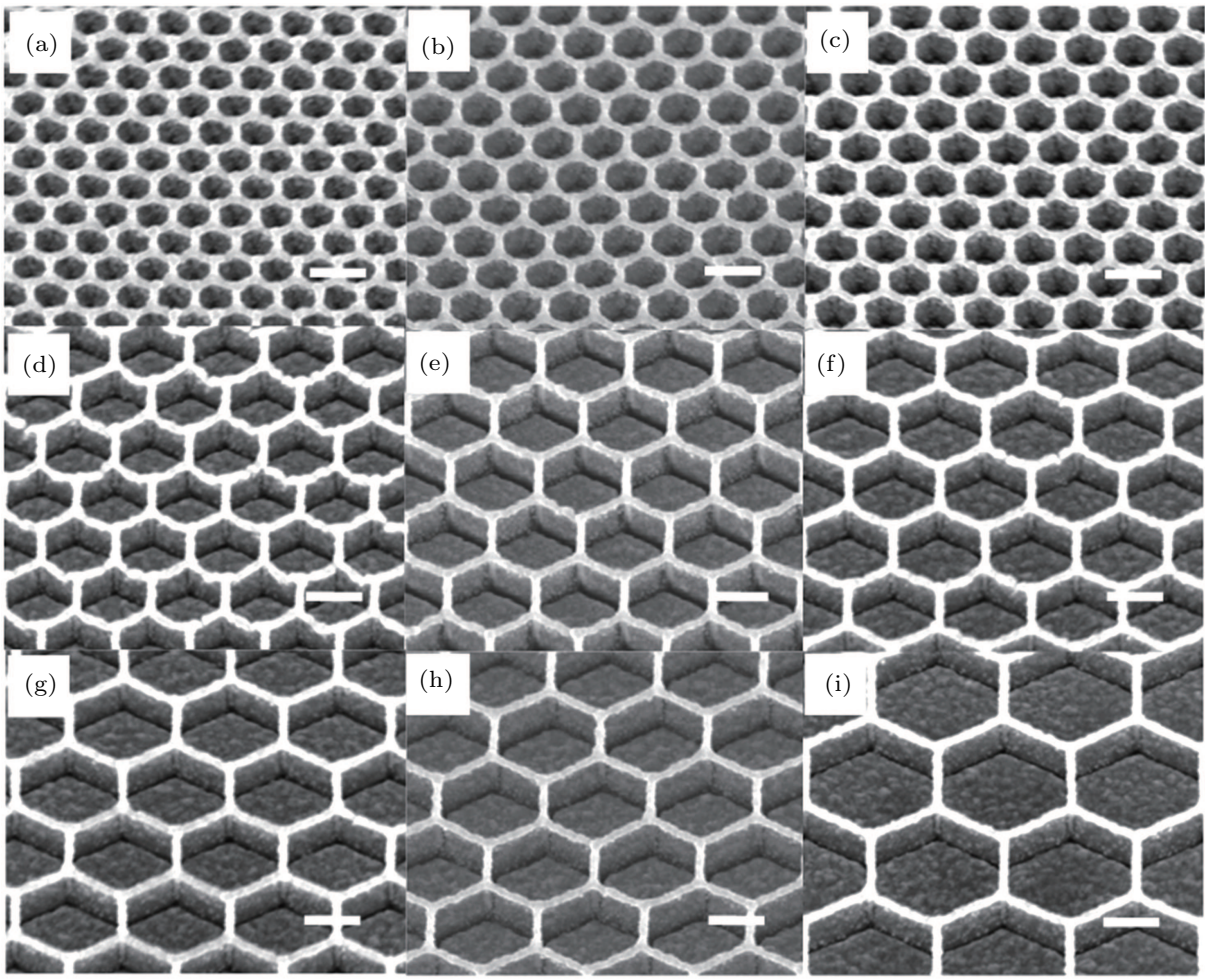


Fig. A3. (color online) Tilt SEM images of hexagonal (5 nm Ag–1 nm Au)-6c/198 nm SiO_2 nanogrids with 87 (a), 101 (b), 105 (c), 157 (d), 188 (e), 194 (f), 227 (g), 274 (h), and 282 nm (i) grid length, respectively. Scale bar: 200 nm.

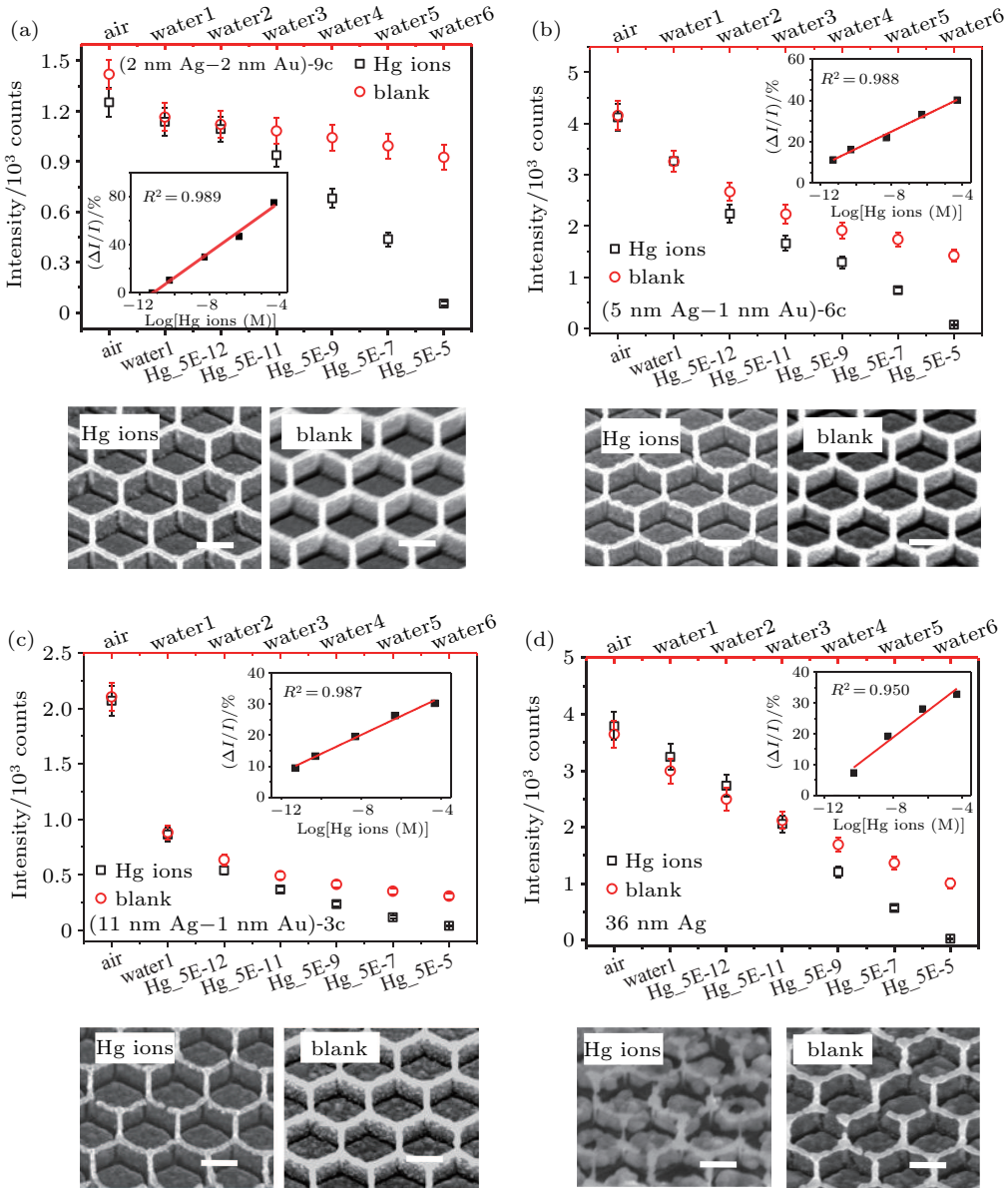


Fig. A4. (color online) Detection of Hg ions by Ag–Au and Ag/198 nm SiO_2nanogrids_h188 probes and their tilt SEM images after measurements. (a) (2 nm Ag–2 nm Au)-9c, (b) (5 nm Ag–1 nm Au)-6c, (c) (11 nm Ag–1 nm Au)-3c, and (d) 36 nm Ag/198 nm SiO_2_h188. Scale bar: 200 nm.

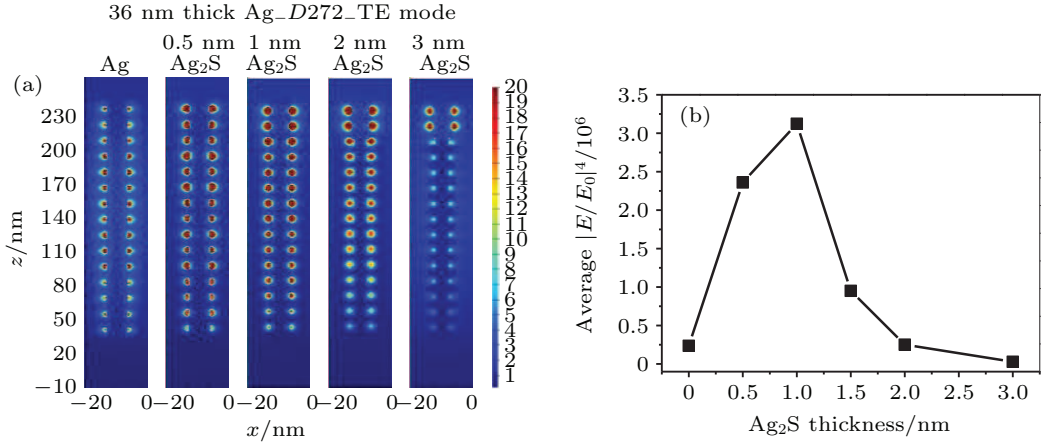


Fig. A5. (color online) (a) Calculated spatial distributions of the electric field intensities at the cross sections of Ag/198 nm SiO_2_D272 nanowalls (244 nm sidewall spacing and 28 nm sidewall width) with different Ag_2S thicknesses for TE mode. (b) The calculated average $|E/E|^4$ of these structures. At the initial stage of exposure, a Ag_2S film as thin as about 1 nm could improve the average electric field enhancement of hot spots dramatically. As the exposure time increases, the thickness of Ag_2S film increased,[32] which would weaken the average electric field enhancement again.

References

[1] Ibáñez-Palomino C, LópezS ánchez J F and Sahuquillo A 2012 *Anal. Chim. Acta* **720** 9

[2] Nolan E M and Lippard S J 2008 *Chem. Rev.* **108** 3443

[3] Kamyabi M A and Aghaei A 2017 *Spectrochim. ActaB* **128** 17

[4] Pelcová P, Dočekalová H and Kleckerová A 2015 *Anal. Chim. Acta* **866** 21

[5] Zhang X, Specht A J, Weisskopf M G, Weuve J and Nie L H 2016 *Biomarkers* **23** 154

[6] Noël M, Christensen J R, Spence J and Robbins C T 2015 *Sci. Total Environ.* **529** 1

[7] Du Y, Liu R, Liu B, Wang S, Han M Y and Zhang Z 2013 *Anal. Chem.* **85** 3160

[8] Zheng P, Li M, Jurevic R, Cushing S K, Liu Y and Wu N 2015 *Nanoscale* **7** 11005

[9] Shi Y, Chen N, Su Y, Wang H and He Y 2018 *Nanoscale* **10** 4010

[10] Fan C Z, Zhu S M and Xin H Y 2017 *Chin. Phys. B* **26** 023301

[11] Wang Y, Wang M, Shen L, Zhu Y, Sun X, Shi G, Xu X, Li R and Ma W 2018 *Chin. Phys. B* **27** 017801

[12] Le Ru E C and Etchegoin P G 2006 *Chem. Phys. Lett.* **423** 63

[13] Li W Q, Wang G, Zhang X N, Geng H P, Shen J L, Wang L S, Zhao J, Xu L F, Zhang L J, Wu Y Q, Tai R Z and Chen G 2015 *Nanoscale* **7** 15487

[14] Leem J, Wang M C, Kang P and Nam S 2015 *Nano Lett.* **15** 7684

[15] Wang X, Wang Y, Cong M, Li H, Gu Y, Lombardi J R, Xu S and Xu W 2013 *Small* **9** 1895

[16] Tabatabaei M, Najiminaini M, Davieau K, Kaminska B, Singh M R, Carson J J L and Lagugné-Labarthet F 2015 *ACS Photon.* **2** 752

[17] Yang Y, Shi J, Kawamura G and Nogami M 2008 *Scr. Mater.* **58** 862

[18] Rycenga M, Hou K K, Cobley C M, Schwartz A G, Camargo P H C and Xia Y 2009 *Phys. Chem. Chem. Phys.* **11** 5903

[19] Fan M, Lai F J, Chou H L, Lu W T, Hwang B J and Brolo A G 2013 *Chem. Sci.* **4** 509

[20] Kim J Y, Kim H, Kim B H, Chang T, Lim J, Jin H M, Mun J H, Choi Y J, Chung K, Shin J, Fan S and Kim S O 2016 *Nat. Commun.* **7** 12911

[21] Nie S and Emory S R 1997 *Science* **275** 1102

[22] Fu Q, Zhan Z, Dou J, Zheng X, Xu R, Wu M and Lei Y 2015 *ACS Appl. Mater. Interfaces* **7** 13322

[23] Kim G, Kim M, Hyun C, Hong S, Ma K Y, Shin H S and Lim H 2016 *ACS Nano* **10** 11156

[24] Qiao X, Su B, Liu C, Song Q, Luo D, Mo G and Wang T 2018 *Adv. Mater.* **30** 1702275

[25] Tian Y, Wang H, Yan L, Zhang X, Falak A, Guo Y, Chen P, Dong F, Sun L and Chu W 2018 arXiv: 1806.02522

[26] Yang C C and Chen W C 2002 *J. Mater. Chem.* **12** 1138

[27] Siegfried T, Ekinci Y, Martin O J F and Sigg H 2013 *ACS Nano* **7** 2751

[28] Khosroabadi A A, Gangopadhyay P, Cocilovo B, Makai L, Basa P, Duong B, Thomas J and Norwood R A 2013 *Opt. Lett.* **38** 3969

[29] Ung B and Sheng Y 2007 *Opt. Express* **15** 1182

[30] Yao W, Liu S, Liao H, Li Z, Sun C, Chen J and Gong Q 2015 *Nano Lett.* **15** 3115

[31] Raether H 1988 *Surf. Plasmons Smooth Surfaces* (Berlin: Springer) pp. 4–6

[32] Bennett H E, Peck R L, Burge D K and Bennett J M 1969 *J. Appl. Phys.* **40** 3351

[33] Santiago-Rodriguez Y, Herron J A, Curet-Arana M C and Mavrikakis M 2014 *Surf. Sci.* **627** 57

[34] Clarebrough L M, Hargreaves M E and West G W 1955 *Proc. R. Soc. Lond. A* **232** 252

[35] Luo Y, Li K, Wen G, Liu Q, Liang A and Jiang Z 2012 *Plasmonics* **7** 461

[36] Ma Y, Liu H, Qian K, Yang L and Liu J 2012 *J. Colloid Interface Sci.* **386** 451

[37] Lv M Y, Teng H Y, Chen Z Y, Zhao Y M, Zhang X, Liu L, Wu Z, Liu L M and Xu H J 2015 *Sens. Actuators B Chem.* **209** 820

[38] Lin D, Wu Z, Li S, Zhao W, Ma C, Wang J, Jiang Z, Zhong Z, Zheng Y and Yang X 2017 *ACS Nano* **11** 1478